Applied Surface Science 598 (2022) 153852

Contents lists available at ScienceDirect

Applied Surface Science

journal homepage: www.elsevier.com/locate/apsusc

Full Length Article

Characteristics of MgO-based sorbents for CO_2 capture at elevated temperature and pressure

Hua Pang [1], Haoran Xu [1], Anwei Sun, Gang Xiao *

State Key Laboratory of Clean Energy Utilization, Zhejiang University, 38 Zheda Road, Hangzhou 310027, China

ARTICLE INFO

Keywords:
CO_2 sorption
MgO-based sorbent
Elevated operating condition
Cyclic stability
Density functional theory

ABSTRACT

MgO-based sorbents are promising candidates for precombustion CO_2 capture performed at elevated temperature and pressure in thermodynamics, where the development of efficient sorbents is of great importance. Herein, we report MgO-Na_2CO_3-KNO_3 sorbents with fast sorption kinetics, high capture capacity and good cyclic stability at elevated conditions. The effects of nitrate species, Na_2CO_3 doping amounts and sorption conditions on the MgO conversion were investigated during cyclic test. In comparison with $LiNO_3$ and $NaNO_3$, the sample with KNO_3 possesses the highest MgO conversion, which increases from 0.78 to 0.86 after 30 cycles with sorption at 400 °C, 2 MPa. For nitrate-promoted MgO, Na_2CO_3 plays an essential role in the initial fast sorption rate. The sorbent with 60 mol%Na_2CO_3 possesses the highest MgO conversion of 0.89 after 30 cycles. Moreover, during the operation range of 400 ℃-480 ℃, 2 MPa, the sorbent exhibits an excellent cyclic stability with porous structure. Density functional theory calculations are further conducted to investigate the mechanism of performance improvement brought by Na_2CO_3. We find dissolved CO_3^{2-} ions will provide chemisorption sites through the formation of C(CO_2)-O(CO_3^{2-}) bonds and can serve as the CO_2 carrier in molten nitrate salts, thus improving both sorption and diffusion rates of CO_2.

1. Introduction

The increasing emission of anthropogenic CO_2 caused by the consumption of fossil fuels is aggravating the climate change [1–4]. Although the share of renewable energy source is continuously increasing to alleviate the depletion of fossil fuels and reduce the CO_2 emission, it is still insufficient to meet the huge energy demand [5,6]. In a shorter term, carbon capture and storage (CCS) from fossil fuels is still the predominant strategy to reduce the CO_2 emission [7]. Among various materials available, solid sorbents have received much attention due to their wide operating temperature range, less waste generation and easy disposal [8,9]. However, the choice of intermediate-temperature solid sorbent is limited, mainly including layered double hydroxides and MgO [10].

MgO is considered to be promising due to its high theorical capture capacity, wide availability in nature and low regeneration energy requirement [8,11–13]. However, the pure MgO showed a low CO_2 capture capacity of ∼ 2 wt%, which is mainly attributed to its lower surface area and the formation of a rigid and CO_2-impermeable product layer [14]. To increase the exposure density of basic site, various strategies have been adopted to increase the surface area of MgO, including decreasing the particle size, synthesizing porous MgO using different magnesium precursors and preparation methods and dispersing MgO on porous supports [15,16]. Although increasing the exposure of basic site is an efficiency strategy to enhance the CO_2 capture capacity, it is still remains to be improved. Recent studies of the MgO-based sorbent have focused on doping with alkali metal salts, among which alkali nitrates/nitrites are usually used as promoters to enhance the CO_2 capture capacity by preventing the formation of the rigid product layer [17–19].

Although the molten nitrate/nitrite promoter could dramatically enhance the CO_2 capture capacity of the MgO-based sorbent, most of the nitrate doped MgO sorbents reported so far suffer from a slow sorption rate at the beginning stage [20]. For example, the (Li-Na-K)NO_3 coated MgO possessed a high and stable CO_2 uptake of about 0.3 $g_{CO2}\ g^{-1}_{sorbent}$ over 40 cycles, but its initial sorption rate was extremely slow, whose CO_2 uptake was about 0.015 $g_{CO2}\ g^{-1}_{sorbent}$ after 6 min of reaction [18]. Recently, the addition of $CaCO_3$ to alkali metal salt-MgO was found to enhance the initial sorption rate, but the mechanism is still under

* Corresponding author.
E-mail address: xiaogangtianmen@zju.edu.cn (G. Xiao).
[1] These authors contributed equally to this paper

https://doi.org/10.1016/j.apsusc.2022.153852
Received 13 March 2022; Received in revised form 20 May 2022; Accepted 28 May 2022
Available online 6 June 2022

discussion. Cui et al. suggested the rapid formation of double carbonate leaded to the improved initial sorption rate [21]. Jin et al. thought the improved sorption rate was related to the Ca ions, which affected the textural property, the lattice parameter and the basicity of the sorbents [22]. Indeed, apart from the cation, the anion is also an important factor that influences the CO_2 adsorption capacity since it plays an essential role in the sorption and the diffusion process, but it was ignored. Moreover, besides the initial sorption rate, the addition of carbonate could influence the cyclic stability [10]. The sorbents always suffered from a rapid decay in CO_2 capture capacity during the cyclic tests when it was conducted under severe conditions [10,23]. Therefore, we broaden the doping amounts of carbonates to investigate whether the increasing addition of carbonates could inhibit the sintering when the sorption was conducted under severe conditions.

MgO-based materials are promising for pre-combustion CO_2 capture processes, which is generally performed at high temperature and pressure. For example, in the Integrated Gasification Combined Cycle (IGCC) plants, the shifted gas from the water–gas shift reactor is in the temperature range of 350–550 ℃ with CO_2 concentration of 15–60 mol% in a total pressure of 2–7 MPa [1,24], which makes MgO-based materials theoretically possible for such operation from thermodynamic equilibrium, but in practical application, the CO_2 capture capacity is always far below the theoretical value due to the limitation of reaction kinetics, which means that the actual CO_2 capture capacity of MgO-based materials and appropriate operation parameter range should be identified by the experiment conducted at elevated temperature and pressure. However, most of the test conditions are in the range of medium temperature (325–375 ℃) and atmospheric pressure [25]. The detailed performance investigation under elevated conditions is missing.

Besides the operation parameter exanimation, another concern is the nitrate promoter, which is effective with a molten state. Although it has been reported that for single nitrate promoted MgO samples, $NaNO_3$ doped MgO sample exhibited the highest CO_2 capture capacity due to the higher solubility of MgO in $NaNO_3$ [26], differences in the CO_2 uptake of nitrate and carbonate co-doped MgO between different nitrate promoters have not been systematically investigated and explained yet. Different from nitrate doped MgO, where the molten nitrate only influences the reaction between MgO and CO_2, for the nitrate and carbonate co-doped MgO, the nitrates not only influence the solubility of MgO but also the carbonates, where the reaction process is more complex. Hence, the systematical study of various single nitrates is of interest as it would help to further understand the performance enhancement mechanism.

In this work, the molten nitrates are selected as additives for MgO. To enhance the initial sorption rate, Na_2CO_3 is further added into the nitrate-promoted MgO material. The CO_2 capture performance of MgO-Na_2CO_3-nitrate are systematically investigated at 360–520 °C and 0.5–3 MPa aiming at confirming the operating temperature range under different CO_2 pressure. Moreover, the effects of nitrate species, doping amounts of Na_2CO_3 and sorption conditions on the cyclic stability were investigated. In addition to the experimental study, density functional theory (DFT) calculations are conducted to explore the interaction mechanism between the CO_2 and anions in the high temperature melting ion liquid.

2. Experimental and computational

2.1. Materials

Magnesium oxide (MgO, GR) and lithium nitrate ($LiNO_3$, AR, 99%) were purchased from Shanghai Macklin Biochemical Co., Ltd. Potassium nitrate (KNO_3, AR, ≥99.0%) and sodium nitrate ($NaNO_3$, AR, ≥99.0%) and sodium carbonate (Na_2CO_3, AR, ≥99.8%) were purchased from Sinopharm Chemical Reagent Co., Ltd.

2.2. Material preparation

MgO-Na_2CO_3-Nitrates was prepared by the wet-mixing method. 2 g of MgO and desired amounts of Na_2CO_3 and nitrate were directly mixed in 30 ml of deionized water. The obtained liquid mixture was stirred in a magnetic stirrer at 35 °C for 0.5 h, after which the mixture was treated by using ultrasonic vibration for 0.5 h. Finally, the liquid slurry was dried in the oven at 120 °C for 6 h and then calcinated in the tubular furnace at 500 °C for 3 h in N_2.

2.3. Experimental apparatus

A schematic diagram of the high-pressure reactor unit is shown in Fig. 1. It consisted of a pneumatic booster pump, a preheating furnace and a high-pressure reactor. The high-pressure reactor was a custom-made nickel-based alloy tubular reactor with outer and inner dimeters of 70 and 40 mm, respectively, and it was placed in a three-zone electric heating furnace with a heating section length of 600 mm. The temperature of the high-pressure reactor was controlled with a proportional integral-derivative (PID) controller during each run. An Omega K-type thermocouple was fixed at the central position inside the reactor, which measured the temperature of the container as the reaction temperature. The pressure of the reactor was maintained by a backpressure regulator. The reaction time was determined using a stopwatch. To prolong the heating time of the reactant gas, the annular coiled tube structure was used in both the preheating furnace and high-pressure reactor. Moreover, the pipeline between the preheating furnace and the high-pressure reactor was insulated by using electric tracing band. The cycling stability test was performed with carbonation in the high-pressure reactor as shown in Fig. 1 and de-carbonation in an atmospheric tubular reactor.

All the samples were pre-calcined at 500 °C for 3 h in a pure N_2 atmosphere to remove the adsorbed gas before the CO_2 sorption test during each run. The test was initiated by setting the backpressure regulator to the predetermined value and then heating the reactor to the desired temperature. After the steady state was obtained, the solid reactant of approximately 0.4 g was loaded and tiled it in a container. Then the ball valve was opened and the container was pushed into the reactor until it touched the thermocouple located in the center of the reactor. After that, the ball valve was closed and the CO_2 gas was fed into the reactor until the pressure reached the desired value. After the predetermined time was achieved, the reactant gas CO_2 was expelled. The sample was taken out quickly and weighed by a delicate electronic balance. The MgO conversion and the CO_2 capture capacity of the sorbents was calculated using the following equations:

$$\text{MgO conversion} = ((m - m_0)/(m_0 \times \omega_{\text{MgO}}))/(M_{\text{CO}_2}/M_{\text{MgO}}) \quad (1)$$

$$\text{CO2 capture capacity} = (m - m_0)/m_0, \text{gCO2/gsorbent} \quad (2)$$

where m_0 and m represent the initial mass of the sample and the mass of sample after carbonation. ω_{MgO} denotes the mass fraction of MgO in the sample, M_{MgO} and M_{co_2} represent the molar mass of MgO and CO_2.

2.4. Characterization

The X-ray diffraction (XRD, PANalytical B.V. X-pert Power) analysis of the sample was performed using an X-ray diffractometer operated at 40 KV and 40 mA with Cu-Kα radiation (λ = 1.5406 Å). The XRD patterns were recorded from 20° to 80° (2θ) with a step size of 0.02°. The morphology of the samples was analyzed by a Scanning Electron Microscope (SEM, HITACHI SU-8010), and the detailed structure and elemental mapping were analyzed using a transmission electron microscopy (TEM, HITACHI, HT7700 EXALENS) equipped with an energy dispersive X-ray spectroscopy (EDS).

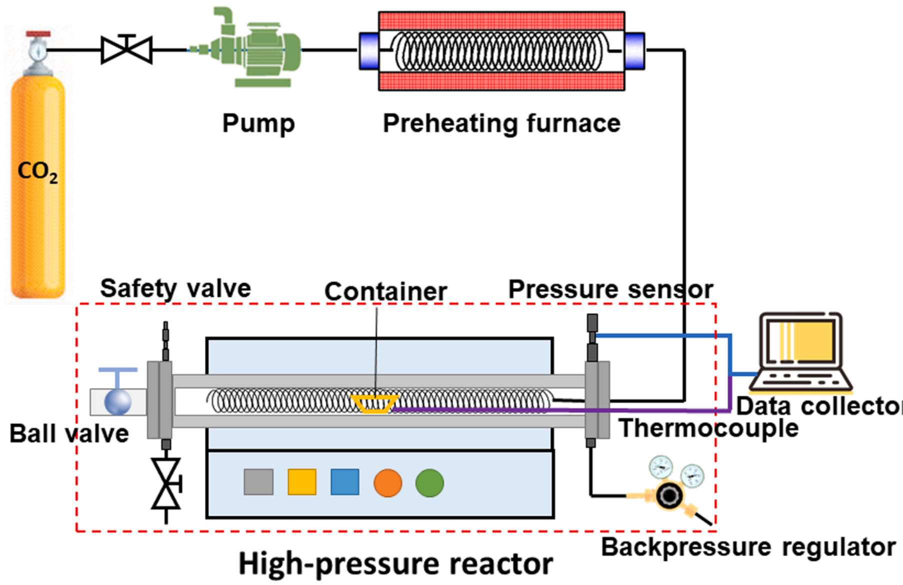

Fig. 1. Diagram of the high-pressure reactor.

2.5. Computational section

To investigate the interaction mechanism between CO_2 and the high temperature melting ionic liquid, DFT calculations were carried out using the Dmol3 package of Material Studio software. The geometry optimizations were performed using the Generalized Gradient Approximation (GGA), Perdew-Burke-Ernzerhof (PBE) functional. All electron core treatment and double numerical plus polarization (DNP) basis set were employed [27–29]. To evaluate the electronic interaction between melting ionic liquid surface and the adsorbed CO_2 molecules, Mulliken charges analysis was performed.

The adsorption energy is used to evaluate the interaction strength between the substrate and adsorbate. For the adsorption of CO_2 on the surface of the high temperature melting ionic liquid, it is defined as the following equation:

$$E_{ads} = (E_{\mathrm{ion+CO2}} - (E_{\mathrm{ion}} + nE_{\mathrm{CO2}}))/n \tag{3}$$

where E_{CO2} and E_{ion} represent the energy of one CO_2 molecule and the melting ion after geometry optimization and $E_{\mathrm{ion+CO2}}$ denotes the total energy of the CO_2 adsorbed on the melting ion. According to the equation, a negative adsorption energy value corresponds to a stable configuration.

3. Results and discussion

3.1. Experimental tests

In the experimental section, the effects of doping amounts of Na_2CO_3 and KNO_3 on the MgO conversion were first investigated at a constant operating condition. Then the effects of various operating pressure and temperature were compared and cyclic tests were performed. The CO_2 uptake results for all figures have been added in the supplementary file.

3.1.1. Effects of doping amounts

Fig. 2(a) shows the effects of KNO_3 doping amounts on the MgO conversion, where a dramatic increase of MgO conversion is observed with the KNO_3 doping. The highest MgO conversion (0.78) is obtained in the case with 20 wt%KNO_3, which was much higher than that without KNO_3 doping (0.32). With the further increase of KNO_3 amount to 35 wt %, the MgO conversion decreases to 0.67. Furthermore, the MgO conversion increased quickly from 0.1 to 0.56 in the first 4 min when the content of KNO_3 increased from 0 to 10 wt%, indicating a significant improvement of the initial CO_2 sorption rate could be achieved with KNO_3 doping.

Fig. 2(b) shows the effects of Na_2CO_3 doping amounts on the MgO

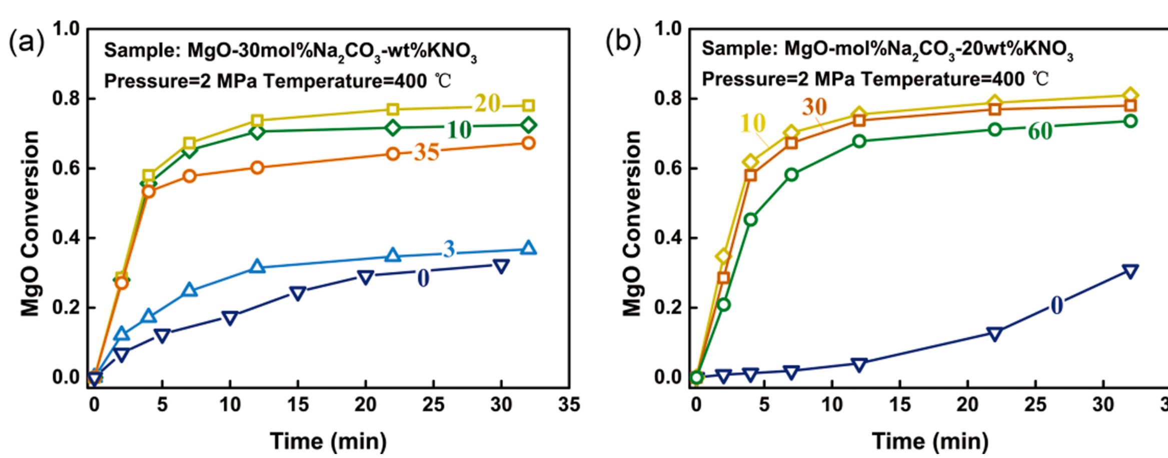

Fig. 2. (a) MgO conversion of MgO-30 mol%Na_2CO_3- wt%KNO_3 at 400 °C, 2 MPa in pure CO_2 with different amounts of KNO_3, (b) MgO conversion of MgO- mol% Na_2CO_3-20 wt%KNO_3 at 400 °C, 2 MPa in pure CO_2 with different amounts of Na_2CO_3.

conversion, where long induction periods are observed for the MgO-mol %Na_2CO_3-20 wt%KNO_3 samples without Na_2CO_3 doping. With the addition of Na_2CO_3, significant increases of the MgO conversion in the beginning stage and the final stage are observed, among which the sample with 10 mol%Na_2CO_3 content shows the best performance. Compared with the sample without Na_2CO_3 doping, the sample with 10 mol%Na_2CO_3 content shows a much higher MgO conversion with the MgO conversion rising from 0.01 to 0.62 in the first 4 min and from 0.31 to 0.81 after 32 min. With the further increase of Na_2CO_3 amount to 60 mol%, the MgO conversion decreases to 0.45 in the first 4 min and 0.74 after 32 min.

3.1.2. Operating condition examination

To examine the effects of operating temperature and pressure, the MgO conversion of MgO-30 mol%Na_2CO_3-20 wt%KNO_3 in the range 360–520 ℃ were investigated at pressures of 0.5, 1, 2 and 3 MPa, as shown in Fig. 3. Overall, a low temperature and a high pressure contribute to the fast sorption rate (MgO conversion at beginning stage) and high sorption capacity (MgO conversion at final stage). It should be noted that no MgO conversion was observed at operating conditions of 0.5 MPa & 520 ℃, 0.5 MPa & 480 ℃, and 1 MPa & 520 ℃, because these operating conditions exceeded the equilibrium state and the reverse reaction rate was faster than the forward reaction. The highest MgO conversion of 0.71 in the first 5 min was obtained at 400 ℃, 3 MPa, while the lowest MgO conversion of 0.08 in the first 4 min was obtained at 520 ℃, 2 MPa. The highest and lowest MgO conversion after 32 min were also obtained at these two working conditions, where the values were 0.79 and 0.16. At different operating pressures, the fastest sorption rates at the beginning stage were achieved at 360 ℃ at 0.5 and 1 MPa, which increased to 400 ℃ at 2 and 3 MPa. The highest sorption capacity at the final stage was achieved at 360 ℃ at 0.5 MPa, and was increased to 400 ℃ at 1, 2 and 3 MPa. The difference of sorption capacity at low temperatures (360–400 ℃) varies slightly with the pressure change, while that at high temperatures (440–520 ℃) was significantly improved with the increase of pressure.

3.1.3. Cyclic test

The cyclic stability of MgO-Na_2CO_3 doped with different species of single molten nitrate was examined through repeated sorption and desorption process with sorption at 400 °C, 2 MPa in pure CO_2 for 30 min and release at 1 bar, 475 °C in pure N_2 for 25 min. The effects of doping nitrates were first investigated as shown in Fig. 4(a), where all the samples performed excellent cyclic stability. Among the samples, MgO-Na_2CO_3-KNO_3 had the best performance, which started with a MgO conversion of 0.78 and achieved 0.86 after 30 cycles. Slight decreases of MgO conversion were observed in the samples with $NaNO_3$ and $LiNO_3$ doping, whose MgO conversions decreased from 0.68 and 0.49 to 0.62 and 0.44 after 30 cycles, respectively.

After confirming the use of KNO_3 as dopant, the amounts of KNO_3 and Na_2CO_3 were adjusted and the related cyclic stability was tested as shown in Fig. 4(b) and (c). From Fig. 4(b), significant increase of MgO conversion occurred when the KNO_3 doping amount increased from 10 wt% to 20 wt%. In contrast to the low MgO conversion of 0.7 after 30 cycles with 10 wt%KNO_3 doping, the MgO conversion of the sample with 20 wt%KNO_3 doping increased to 0.86. Further increase in the KNO_3 doping amount to 35 wt% did not lead to additional increase in MgO conversion, whose MgO conversion decreased slightly to 0.85 after 30 cycles. After calculation, the highest CO_2 uptake of 0.42 $g_{CO2}/g_{sorbent}$ was obtained with 20 wt%KNO_3 doping, which was higher than that with low or high KNO_3 doping amounts as shown in Fig. S3(b). This can be explained by that much molten nitrates addition easily leads to sintering and a low surface area [30].

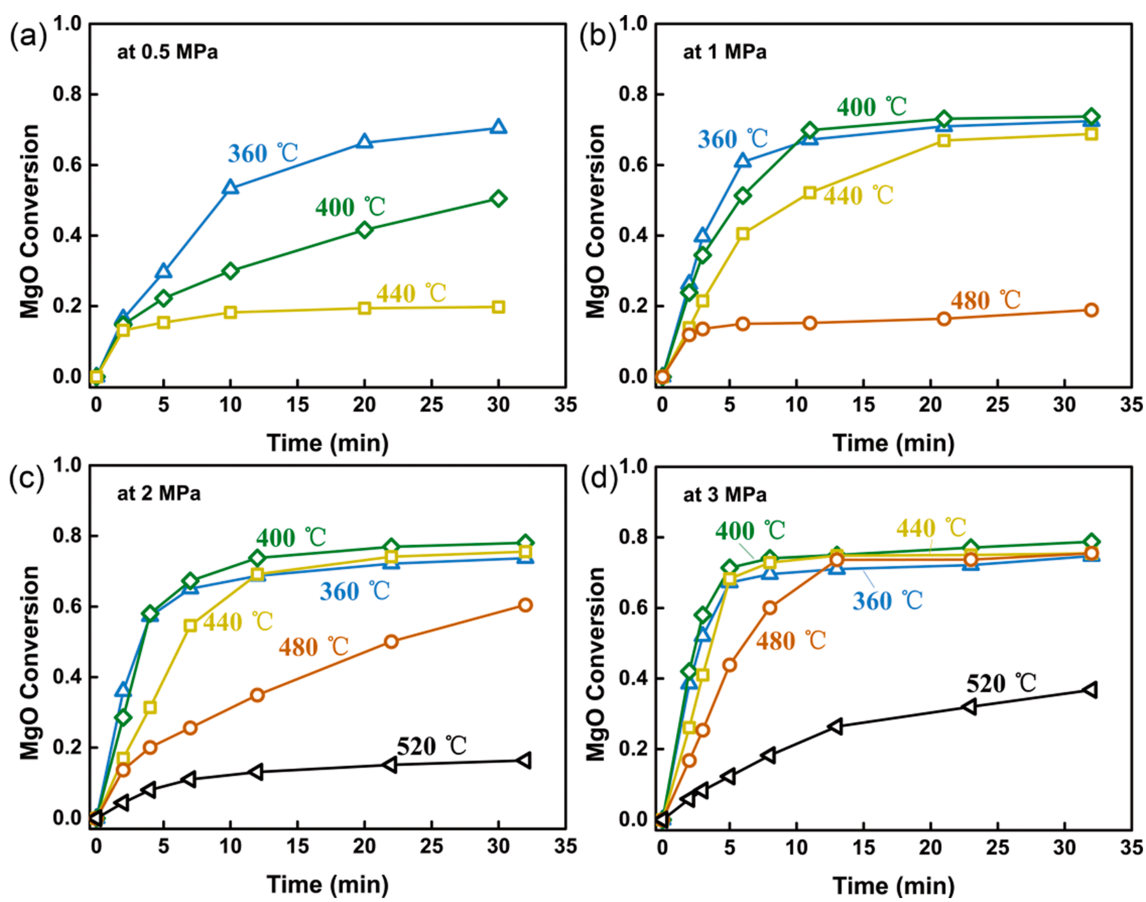

Fig. 3. MgO conversion of MgO-30 mol%Na_2CO_3-20 wt%KNO_3 with different sorption temperatures in pure CO_2. (a) at 0.5 MPa; (b) 1 MPa; (c) 2 MPa; (d) 3 MPa.

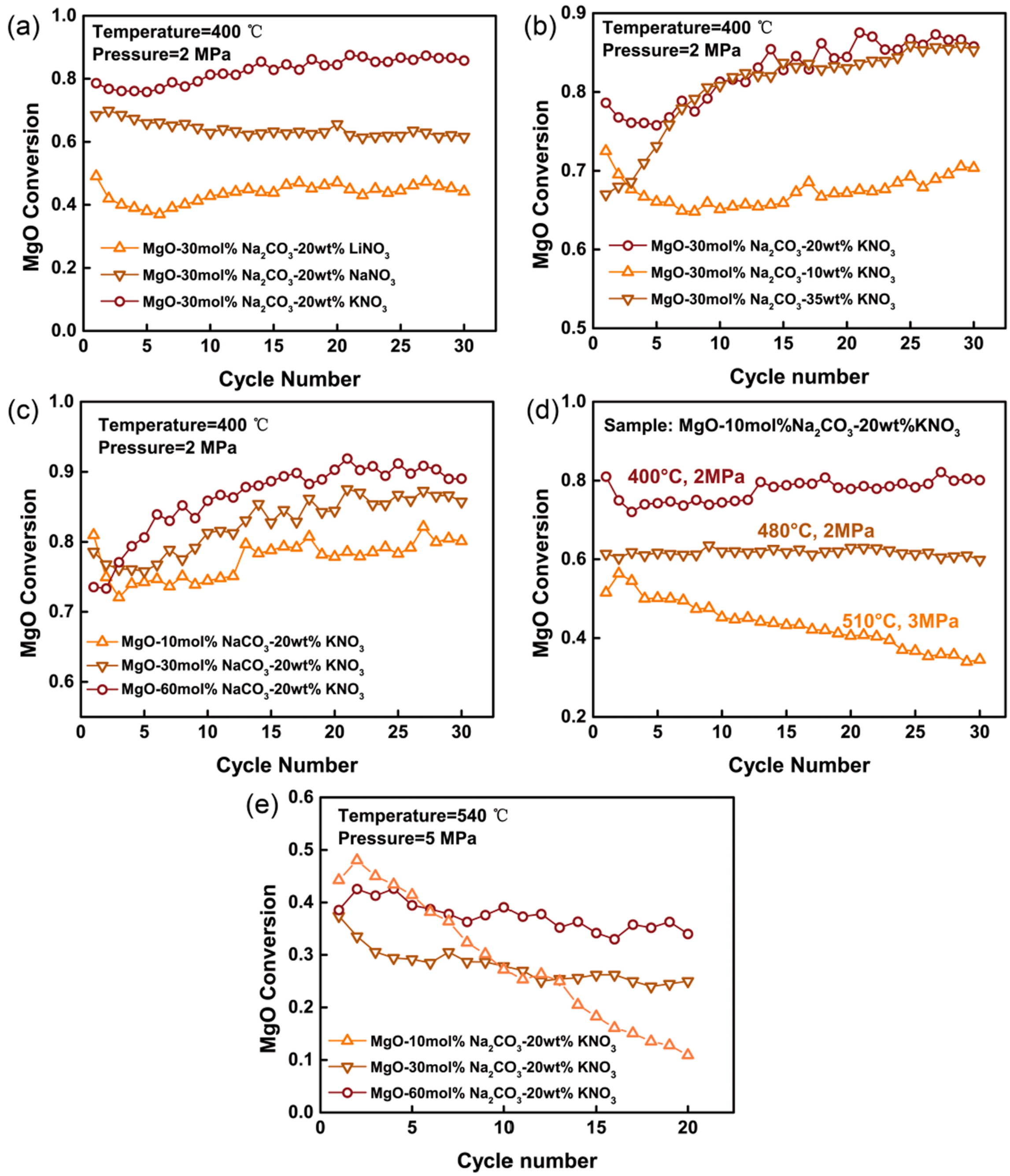

Fig. 4. Cyclic test of samples with sorption at 400 °C, 2 MPa in pure CO_2 for 30 min and desorption at 475 °C, 1 bar in pure N_2 for 25 min, (a) with different species of single molten nitrate, (b) with different amounts of KNO_3 and (c) with different amounts of Na_2CO_3 after 30 cycles; (d) cyclic test of MgO-10 mol%Na_2CO_3-20 wt% KNO_3 under various sorption conditions; (e) with different amounts of Na_2CO_3 after 20 cycles at 540 ℃, 5 MPA.

The amount of Na_2CO_3 was further adjusted and the related cyclic stability was further tested as shown in Fig. 4(c). The increase of Na_2CO_3 was found to decrease the MgO conversion in the first cycle but contributed to the rise of MgO conversion in the following cycles. As a result, the sample with 60 mol% Na_2CO_3 doping started with a MgO conversion of 0.73 and reached 0.89 after 30 cycles. For comparison, the sample with 10 mol% Na_2CO_3 doping started with a MgO conversion of 0.81 but decreased to 0.8 after 30 cycles. Although the MgO conversion of the sample with 10 mol% Na_2CO_3 is lower than that with higher content of Na_2CO_3, its CO_2 sorption capacity was the highest as shown in Fig. S3(c), which retained 0.56 $g_{CO2}/g_{sorbent}$ after 30 cycles. The CO_2 sorption capacity of MgO-10 mol%Na_2CO_3-20 wt%KNO_3 is higher than the MgO-K_2CO_3 sorbents (~0.12 $g_{CO2}/g_{sorbent}$) with sorption condition of 50 %CO_2-50 %N_2, 2 MPa and 425 °C after 3 cycles [11].

To investigate the effects of operating parameters on the cyclic stability, the MgO-10 mol%Na_2CO_3-20 wt%KNO_3 with the highest CO_2 sorption capacity was selected as the sample and the operating parameter was increased from 400 °C, 2 MPa to 510 °C, 5 MPa as shown in Fig. 4(d). The increase of the operating parameter was found to decrease the MgO conversion during the cyclic test. The sample with operation at mild sorption condition of 400–480 °C, 2 MPa showed a good cyclic stability, whose MgO conversion maintained at 0.8 and 0.6 after 30 cycles, respectively. With increase of operating parameter to 510 °C, 3 MPa, the MgO conversion decreased from 0.52 to 0.34 after 30 cycles. Above tests indicated that the sorption conditions have a significant influence on the cyclic stability. Under severe condition (510 °C, 3 MPa), the MgO conversion decreased obviously with the increasing cyclic number due to the aggravated deactivation.

To investigate the effect of Na_2CO_3 doping amounts on the cyclic stability under severe sorption conditions, a further increase of operating temperature to 540 ℃, 5 MPa was further examined as shown in Fig. 4(e), where a sharp decline of MgO conversion from 0.44 to 0.11 after 20 cycles with 10 mol% Na_2CO_3 doping was observed. The sample with 60 mol% Na_2CO_3 doping showed a good cyclic stability, whose MgO conversion maintained at 0.35 after 20 cycles. Above tests indicated that the deactivation can be alleviated with high amount of Na_2CO_3 doping.

3.2. XRD and microstructure analysis

For MgO-30 mol%Na_2CO_3-20 wt%KNO_3, the time-evolution products after reaction with CO_2 at 400 °C, 2 MPa were investigated by XRD as shown in Fig. 5(a). Before carbonation, Na_2CO_3, MgO and KNO_3 were observed without any recombination components. After 2 min of sorption, many diffraction peaks indexed as $Na_2Mg(CO_3)_2$ emerged, together with a weak $MgCO_3$ peak. After 4 min of sorption, a large number of strong $MgCO_3$ peaks appeared along with a remarkable decrease of the MgO peaks, suggesting the formation of $Na_2Mg(CO_3)_2$ preceded the formation of $MgCO_3$. After the 30th sorption, the peak intensity of $Na_2Mg(CO_3)_2$ increased significantly, but no obvious change of the peak intensity of $MgCO_3$ was observed. Therefore, it can be inferred that the increased MgO conversion in the cyclic test was mainly attributed to the formation of $Na_2Mg(CO_3)_2$.

Although the Na_2CO_3 structure was detected in the fresh sample, the diffraction peaks shifted towards lower 2θ angles compared with the MgO-Na_2CO_3 mixture as shown in Fig. 5(b). For comparison, no shift trace of diffraction peaks of Na_2CO_3 with $NaNO_3$ doping was observed. The lower angles shift was in correspondence with the reduction in the lattice spacing based on the Bragg equation ($2d\sin\theta = n\lambda$), indicating the larger ionic radius of K^{1+} was doped into the Na_2CO_3 lattice [31,32]. The large intensity changes of (2 0 2), (1 1 2), (3 1 0) and (0 0 2) peaks also suggested that KNO_3-doping could lead to the lattice distortion of Na_2CO_3.

The XRD patterns of MgO-Na_2CO_3 doped with $NaNO_3$ and $LiNO_3$ before and after carbonation were further compared as shown in Fig. 5 (c) and (d). Fig. 5(c) revealed that MgO-Na_2CO_3-$NaNO_3$ was comprised of $NaNO_3$, MgO and Na_2CO_3 before carbonation, and the products were indexed as $MgCO_3$ and $Na_2Mg(CO_3)_2$ after carbonation reaction. From Fig. 5(d), before sorption, only MgO and Na_2CO_3 phases were detected in MgO-Na_2CO_3-$LiNO_3$, while $LiNO_3$ phase was not found. Instead of the missing $LiNO_3$ phase, phases indexed as $LiNaCO_3$ and $NaNO_3$ emerged, indicating that the reaction between $LiNO_3$ and Na_2CO_3 occurred during the preheat treatment process. After sorption, $MgCO_3$ and $Na_2Mg(CO_3)_2$ phases were detected. Moreover, the $LiNaCO_3$ phase disappeared along with the appearance of Li_2CO_3, suggesting that the $LiNaCO_3$ decomposed into Li_2CO_3 and Na_2CO_3 during the sorption process, but the Li_2CO_3 did not participate in the carbonation reaction.

From the above XRD analysis, it can be inferred that the higher MgO conversion with KNO_3 dopant compared to $NaNO_3$ may be related to the distorted crystal structure of Na_2CO_3. The distorted crystal structure will lead to more lattice defects of the product layer, which is beneficial to the ionic diffusion and enhance the mass transfer process. In the case of

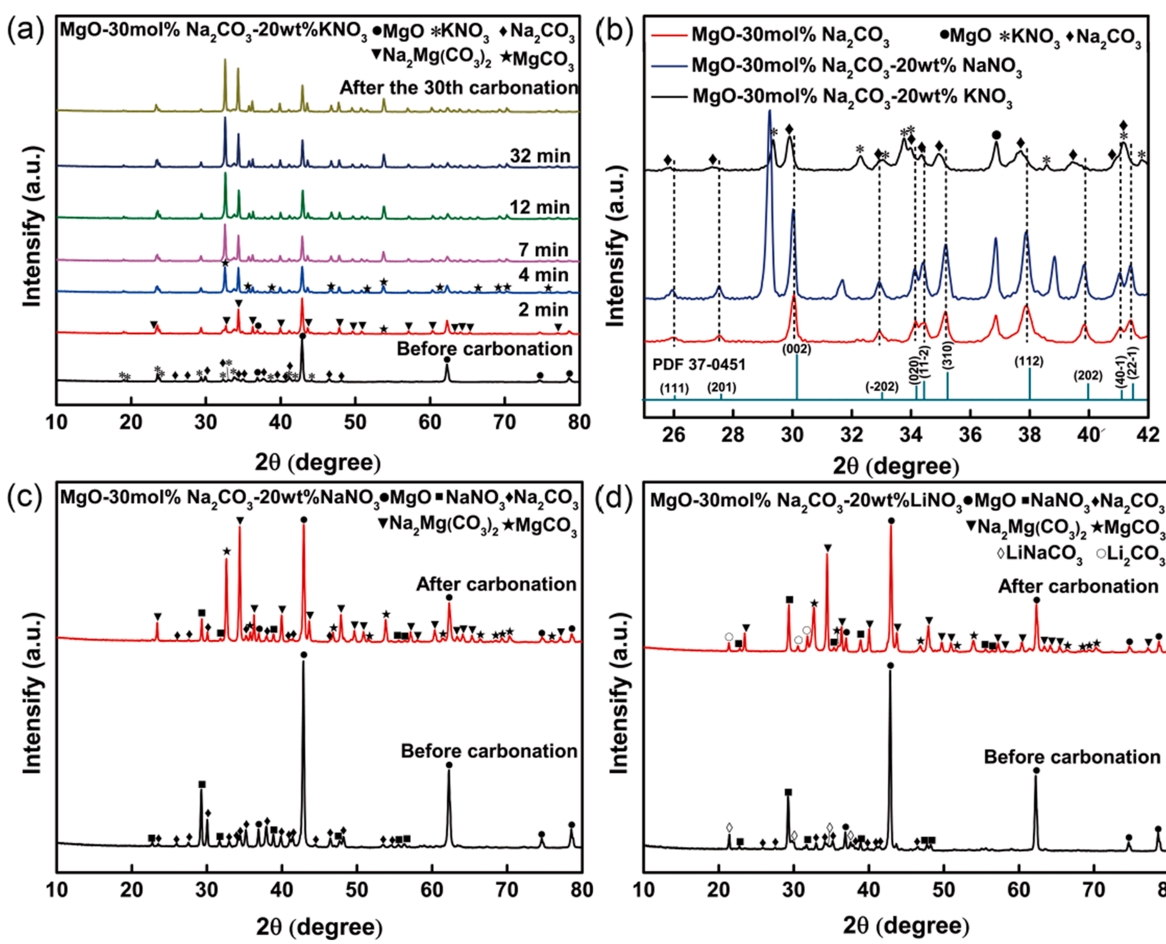

Fig. 5. (a) XRD patterns of MgO-30 mol%Na_2CO_3-20 wt%KNO_3 with various sorption times in pure CO_2 at 400 °C, 2 MPa; (b) details of XRD patterns comparing the peaks of Na_2CO_3 in 25-42° region before reaction; XRD patterns before and after carbonations in pure CO_2 at 400 °C, 2 MPa for 30 min, (c) with $NaNO_3$ and (d) $LiNO_3$.

$LiNO_3$ doing, the $LiNO_3$ reacted with Na_2CO_3 to form $NaNO_3$ and $LiNaCO_3$, which further decomposed to Na_2CO_3 and Li_2CO_3, but the Li_2CO_3 did not participate in the carbonation reaction, leading to a low MgO conversion of MgO-Na_2CO_3-$LiNO_3$ compared with MgO-Na_2CO_3-KNO_3 and MgO-Na_2CO_3-$NaNO_3$.

The cyclic stability was strongly affected by the microstructure of material during the cyclic test. To clarify the microstructural evolution with different sorption conditions, morphologies of the MgO-10 mol% Na_2CO_3-20 wt%KNO_3 after multi cycles with different sorption conditions (400 °C, 2 MPa, 480 °C, 2 MPa and 510 °C, 3 MPa) were analyzed. The raw sample was composed of small particles, with an average particle size of 193 nm as calculated by the image processing program (ImageJ) as shown in Fig. 6(a). In 30 cycles with sorption at 400 °C, 2 MPa and 480 °C, 2 MPa, both of the samples exhibited porous structures with coalescence of small particles, as shown in Fig. 6(b) and (c), but it exhibited severe sintering at 510 ℃, 3 MPa, as shown in Fig. 6(d). This explains the decrease of MgO conversion in 30 cycles under the severe condition of 510 ℃, 3 MPa.

TEM and elemental mapping images were analyzed for the MgO-30 mol%Na_2CO_3-20 wt%KNO_3 as shown in Fig. 6(e)-(h). Before reaction, the particle performed a hexagon shape with an uniform distribution of magnesium and sodium elements. However, a huge potassium grain was observed as shown in Fig. 6(h), where the flow of molten potassium nitrate was further observed under the irradiation of electron beam as shown in Fig. 6(i)-(k). With the flow of molten nitrates, the homogenization of potassium distribution will be improved, which may be contributed to the increase of the MgO conversion in the cyclic test under the mild condition of at 400 ℃ and 2 MPa.

The pore characteristics were analyzed by N_2 adsorption/desorption isotherms. As shown in Table 1, the BET surface area of the MgO-10 mol %Na_2CO_3-20 wt%KNO_3 decreased significantly from 4.38 to 0.69 m^2/g after 20 cycles at 540 ℃, 5 MPa. For comparison, the surface area of the sample with higher Na_2CO_3 content of 30 mol% increased slightly from 2.11 to 2.49 m^2/g. The N_2 adsorption/desorption isotherms and pore-diameter distribution were shown in Fig. 7. It was found that the pore of MgO-10 mol%Na_2CO_3-20 wt%KNO_3 almost disappeared, indicating

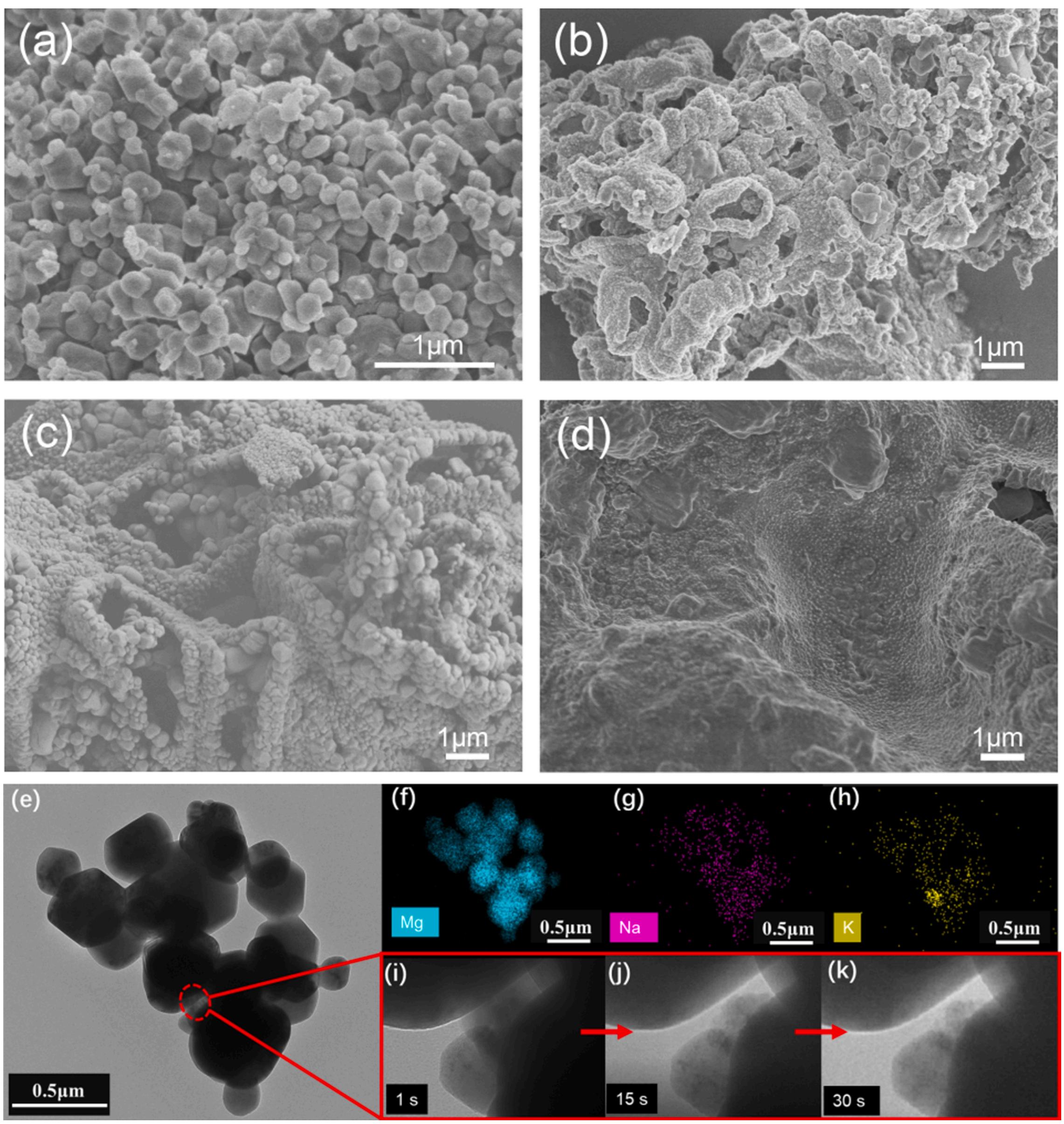

Fig. 6. Morphology of MgO-10 mol%Na_2CO_3-20 wt%KNO_3 with sorption at different conditions, (a) fresh sample, desorption morphology with different sorption conditions, (b) at 400 °C, 2 MPa, (c) at 480 °C, 2 MPa and (d) 510 °C, 3 MPa. TEM and elemental mapping images of MgO-30 mol%Na_2CO_3-20 wt%KNO_3, (e) TEM image, (f)-(h) EDS elemental mapping images and (i)-(k) time evolution of the potassium grain.

Table 1
Textual properties of samples before and after cyclic tests.

Samples	BET surface area [m^2/g]	BJH pore volume [cm^3/g]
MgO-10 mol%Na_2CO_3-20 wt%KNO_3	4.38	0.0144
MgO-10 mol%Na_2CO_3-20 wt% KNO_3 (540 ℃, 5 MPa, 20 cycle)	0.69	0.00315
MgO-30 mol%Na_2CO_3-20 wt%KNO_3	2.11	0.00575
MgO-30 mol%Na_2CO_3-20 wt% KNO_3 (540 ℃, 5 MPa, 20 cycle)	2.49	0.0129

that severe sintering problem occurred after 20 cycles, while mesopores in the range of 10–100 nm appeared in the sample with 30 mol% Na_2CO_3, which is favorable for carbonation. Thus, the sample with higher Na_2CO_3 content can maintain stable MgO conversion over cycles.

3.3. DFT analysis

To investigate the interaction mechanism between the CO_2 and the melted ion liquid, DFT calculations were conducted in this section. The anion components of the melted ion liquid were first determined since they are important factors to influence the CO_2 adsorption capacity. As analyzed through the endothermic peaks of DSC profile [33], part of the carbonates could be dissolved in molten nitrates, therefore, the anions were assumed to mainly include CO_3^{2-} and NO_3^-.

The optimized configurations of CO_2 molecule adsorption and the related adsorption geometry, energy and Mulliken charges are presented in Fig. 8 and Table 2, respectively. The C atom of CO_2 was found to be adsorbed on the O atom of CO_3^{2-}, where the C(CO_2)-O(CO_2) bond changed from the both double bonds (O = C = O) to the partial double bond (O-C = O) after CO_2 adsorption on CO_3^{2-} and a new ionic bond with a bond length of 1.467 Å was formed between C(CO_2) and O(CO_3^{2-}). However, no bond was formed when the CO_2 reacted with NO_3^-, where the distance between the C(CO_2) and O(NO_3^-) was 2.433 Å. Besides, there was 0.708 e transferred from CO_3^{2-} to CO_2, which was 7 times higher than the value from NO_3^-. Moreover, the CO_2 adsorption energy of CO_3^{2-} was −2.803 eV, which is approximately 6.31 times higher than the value of CO_2 adsorption on NO_3^-, indicating a more stable configuration of the CO_2 adsorption on CO_3^{2-}.

The stable configuration of two CO_2 molecules adsorption on CO_3^{2-} further presented that the C(CO_2)-O(CO_2) bonds of both CO_2 molecules changed to the partial double bond with the formation of two new C(CO_2)-O(CO_3^{2-}) bonds. The adsorption energy calculated was −2.018 eV, indicating that the two CO_2 molecules were chemically adsorbed on CO_3^{2-} and formed $C_3O_7^{2-}$. From the above results, it can be inferred that CO_3^{2-} plays an essential role in the reaction process, which not only provides the chemisorption site at the initial reaction stage, but also works as CO_2 carrier to transport CO_2 in the melted ion liquid, thus enhancing the CO_2 adsorption and diffusion rates. It should be noted that the existence of $C_2O_5^{2-}$ has been detected in the mixed oxide-ion and carbonate-ion conducting membranes at a CO_2 atmosphere of 1 bar using the in-situ Raman spectroscopy [34].

From the above results, it can be inferred that CO_3^{2-} plays an essential role in the reaction process, which not only provides the chemisorption site at the initial reaction stage, but also works as CO_2 carrier to transport CO_2 in the melted ion liquid, thus enhancing the CO_2 adsorption and diffusion rates.

4. Conclusion

A series of MgO-based sorbents were prepared and tested at various operating conditions for the CO_2 adsorption application at elevated temperature and pressure. Their adsorption rate and capacity were significantly improved by doping proper Na_2CO_3, where the MgO

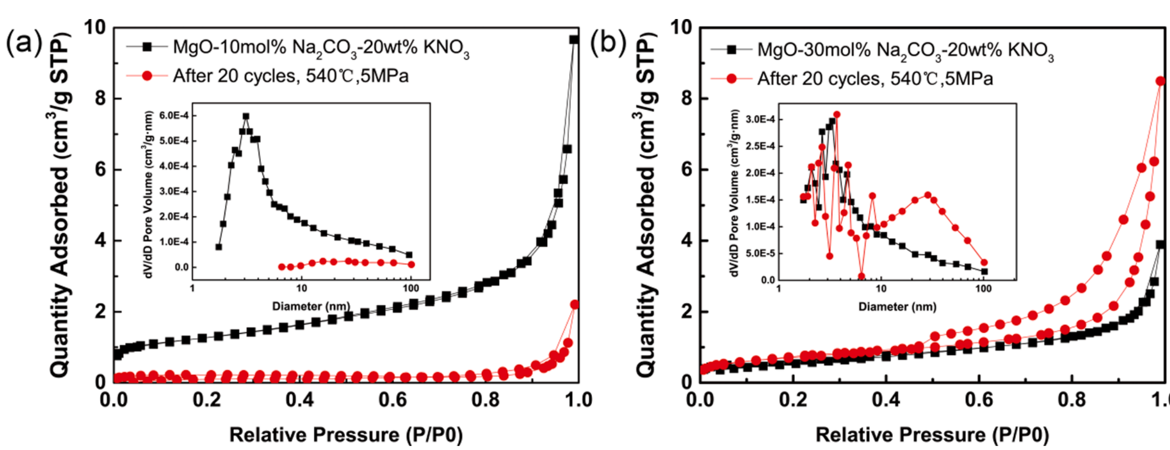

Fig. 7. N_2 adsorption–desorption isotherms and pore-diameter distribution (inset) of samples before and after 20 cycles, (a) MgO-10 mol%Na_2CO_3-20 wt%KNO_3 and (b) MgO-30 mol%Na_2CO_3-20 wt%KNO_3, STP: standard temperature and pressure.

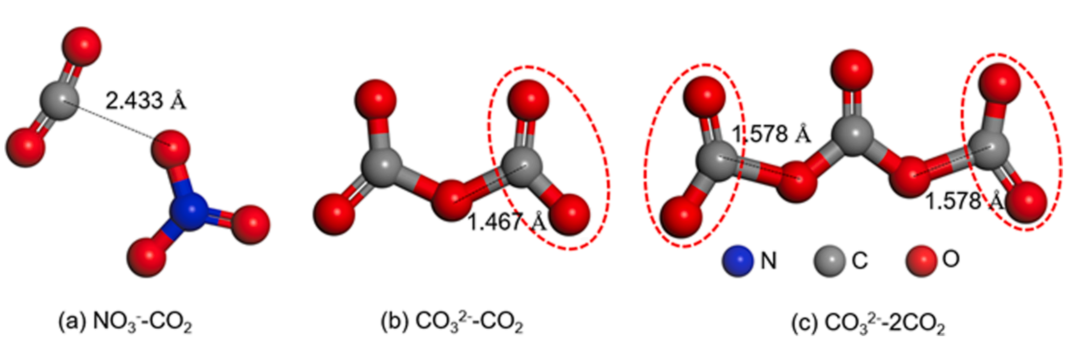

Fig. 8. Geometry configuration of CO_2 adsorption on different ions in the melted ionic liquid.

Table 2
Adsorption geometry, energy and Mulliken atomic charges of CO_2 adsorbed on anion.

Substrate	$d(O_{Substrate} - C_{CO2})$ (Å)	$d(C_{CO2}$-$O_{CO2})$ (Å)	∠CO_2(O-C-O) (°)	E_{ads} (eV)	Q_{CO2} (e)
NO_3^- - CO_2	2.433	1.181/1.185	166.397	−0.444	−0.104
CO_3^{2-} - CO_2	1.467	1.253/1.270	129.140	−2.803	−0.708
CO_3^{2-}- $2CO_2$	1.5781.578	1.234/1.2441.234/1.245	135.053135.042	−2.018−2.018	−0.551−0.552

conversion was raised from 0.01 to 0.62 by doping 10 mol%Na_2CO_3 into MgO-20 wt%KNO_3 at 400 ℃, 2 MPa. That is because Na_2CO_3 dopant not only works as reactant along with MgO to react with CO_2 but also its product $Na_2Mg(CO_3)_2$ serves as catalyst promoting the reaction between MgO and CO_2. DFT calculations revealed that the C atom of CO_2 was chemically adsorbed on the O atom of CO_3^{2-} by forming the C(CO_2)-O (CO_3^{2-}) bond. The addition of CO_3^{2-} not only provided the chemisorption site but also enhanced CO_2 diffusion in the melted ion liquid by serving as the transport carrier. The performance of salt-promoted MgO sorbent was further investigated at various operating temperature and pressure conditions in the range of 360–520 °C and 0.5–3 MPa, where the highest MgO conversion of 0.71 in the first 5 min was obtained at 400 ℃, 3 MPa.

The effects of different single molten nitrates ($LiNO_3$, $NaNO_3$ and KNO_3) on the MgO conversion and the cyclic stability were also compared at 400 °C, 2 MPa. Among all the samples, the one doped with KNO_3 achieved the highest MgO conversion (0.86) after 30 cycles. Through the XRD analysis, the excellent performance was attributed to the distorted crystal structure of Na_2CO_3, which leaded to lattice defects of the product layer and enhanced the ionic diffusion.

The effect of Na_2CO_3 content and sorption conditions on the cyclic stability was further examined. The results indicated that all the samples with different amounts of Na_2CO_3 dopant exhibited increased MgO conversion with the increase of cyclic number at the mild sorption condition of 400 °C, 2 MPa, which was mainly attributed to the enhanced homogenization of molten salt distribution. However, with the increase of the sorption parameter to 510 °C, 3 MPa, the MgO-10 mol %Na_2CO_3-20 wt%KNO_3 exhibited a significant decay in the MgO conversion during the cyclic test due to the sintering problem. To explore the Na_2CO_3 content on the cyclic stability under severe sorption conditions, the test parameter further increased to 540 °C, 5 MPa. The results indicated that a high Na_2CO_3 content was favorable for the cyclic stability due to the growth of a porous structure in the cyclic test, which increased the specific surface area and pore volume and alleviated the sintering problem.

CRediT authorship contribution statement

Hua Pang: Methodology, Software, Validation, Formal analysis, Investigation, Writing – original draft. **Haoran Xu:** Methodology, Software, Validation, Formal analysis, Project administration, Writing – review & editing. **Anwei Sun:** Writing – review & editing, Visualization. **Gang Xiao:** Conceptualization, Methodology, Resources, Data curation, Writing – review & editing.

Declaration of Competing Interest

The authors declare that they have no known competing financial interests or personal relationships that could have appeared to influence the work reported in this paper.

Acknowledgements

The authors gratefully acknowledge the support from the Zhejiang Provincial Natural Science Foundation (NO.LR20E060001), the Innovative Research Groups of the National Natural Science Foundation of China (No.51621005) and Program of Introducing Talents of Discipline to University (111 Program, No. B08026).

Appendix A. Supplementary material

Supplementary data to this article can be found online at https://doi.org/10.1016/j.apsusc.2022.153852.

References

[1] S.G. Subraveti, K.N. Pai, A.K. Rajagopalan, N.S. Wilkins, A. Rajendran, A. Jayaraman, G. Alptekin, Cycle design and optimization of pressure swing adsorption cycles for pre-combustion CO_2 capture, Appl. Energy 254 (2019), 113624, https://doi.org/10.1016/j.apenergy.2019.113624.

[2] T. Zhang, M. Li, P. Ning, Q. Jia, Q. Wang, J. Wang, K_2CO_3 promoted novel Li_4SiO_4-based sorbents from sepiolite with high CO_2 capture capacity under different CO_2 partial pressures, Chem. Eng. J. 380 (2020), 122515, https://doi.org/10.1016/j.cej.2019.122515.

[3] Y. Yang, S. Yao, Y. Hu, J. Sun, J. Cao, Q. Li, W. Liu, Mechanochemically activated Li_4SiO_4-based adsorbent with enhanced CO_2 capture performance and its modification mechanisms, Fuel 273 (2020) 117749.

[4] G. Ji, M.Z. Memon, H. Zhuo, M. Zhao, Experimental study on CO_2 capture mechanisms using Na_2ZrO_3 sorbents synthesized by soft chemistry method, Chem. Eng. J. 313 (2017) 646–654, https://doi.org/10.1016/j.cej.2016.12.103.

[5] E.I. Koytsoumpa, C. Bergins, E. Kakaras, The CO_2 economy: Review of CO_2 capture and reuse technologies, The Journal of Supercritical Fluids 132 (2018) 3–16, https://doi.org/10.1016/j.supflu.2017.07.029.

[6] Z. Zhang, Y. Li, W. Zhang, J. Wang, M.R. Soltanian, A.G.J.R. Olabi, S.E. Reviews, Effectiveness of amino acid salt solutions in capturing CO_2: a review, Renew. Sust. Energ. Rev. 98 (DEC.) (2018) 179–188, https://doi.org/10.1016/j.rser.2018.09.019.

[7] W.L. Theo, J.S. Lim, H. Hashim, A.A. Mustaffa, W.S.J.A.E. Ho, Review of pre-combustion capture and ionic liquid in carbon capture and storage, Appl. Energy 183 (2016) 1633–1663, https://doi.org/10.1016/j.apenergy.2016.09.103.

[8] J. Seongmin, K.o. Kwang-Jun, L. Chang-Ha, Direct formation of hierarchically porous MgO-based sorbent bead for enhanced CO_2 capture at intermediate temperatures, Chem. Eng. J. 371 (2019) 64–77, https://doi.org/10.1016/j.cej.2019.04.020.

[9] H. Lee, M.L.T. Trivino, S. Hwang, S.H. Kwon, S.G. Lee, J.H. Moon, J. Yoo, J.G. Seo, In Situ Observation of Carbon Dioxide Capture on Pseudo-Liquid Eutectic Mixture-Promoted Magnesium Oxide, ACS Appl. Mater. Interfaces 10 (3) (2017) 2414–2422, https://doi.org/10.1021/acsami.7b14256.

[10] H. Cui, Q. Zhang, Y. Hu, C. Peng, X. Fang, Z. Cheng, V.V. Galvita, Z. Zhou, Ultrafast and Stable CO_2 Capture Using Alkali Metal Salt-Promoted MgO-$CaCO_3$ Sorbents, ACS Appl. Mater. Interfaces 10 (24) (2018) 20611–20620, https://doi.org/10.1021/acsami.8b05829.

[11] A. Hassanzadeh, J. Abbasian, Regenerable MgO-based sorbents for high-temperature CO_2 removal from syngas: 1, Sorbent development, evaluation, and reaction modeling, Fuel 89 (6) (2010) 1287–1297, https://doi.org/10.1016/j.fuel.2009.11.017.

[12] S. Zarghami, A. Hassanzadeh, H. Arastoopour, J. Abbasian, Effect of Steam on the Reactivity of MgO-Based Sorbents in Precombustion CO_2 Capture Processes, Ind. Eng. Chem. Res. 54 (36) (2015) 8860–8866, https://doi.org/10.1021/acs.iecr.5b01175.

[13] J. Chi, L. Zhao, B. Wang, Z. Li, Y. Xiao, Y. Duan, Thermodynamic performance assessment and comparison of IGCC with solid cycling process for CO_2 capture at high and medium temperatures, Int. J. Hydrog. Energy 39 (12) (2014) 6479–6491, https://doi.org/10.1016/j.ijhydene.2014.02.005.

[14] P. Li, W. Liu, J.S. Dennis, H.C. Zeng, Synthetic Architecture of MgO/C Nanocomposite from Hierarchical-Structured Coordination Polymer toward Enhanced CO_2 Capture, ACS Appl. Mater. Interfaces 9 (11) (2017) 9592–9602, https://doi.org/10.1021/acsami.6b14960.

[15] Y.Y. Li, M.M. Wan, W.G. Lin, Y. Wang, J.H. Zhu, A novel porous MgO sorbent fabricated through carbon insertion, J. Mater. Chem. A 2 (30) (2014) 12014–12022, https://doi.org/10.1039/c4ta01188k.

[16] Y.Y. Li, M.M. Wan, X.D. Sun, J. Zhou, Y. Wang, J.H. Zhu, Novel fabrication of an efficient solid base: carbon-doped MgO–ZnO composite and its CO2 capture at 473 K, J. Mater. Chem. A 3 (36) (2015) 18535–18545, https://doi.org/10.1039/c5ta04309c.

[17] Y. Qiao, J. Wang, Y. Zhang, W. Gao, T. Harada, L. Huang, T.A. Hatton, Q. Wang, Alkali Nitrates Molten Salt Modified Commercial MgO for Intermediate-Temperature CO_2 Capture: optimization of the Li/Na/K Ratio, Ind. Eng. Chem. Res. 56 (6) (2017) 1509–1517, https://doi.org/10.1021/acs.iecr.6b04793.

[18] T. Harada, F. Simeon, E.Z. Hamad, T.A. Hatton, Alkali Metal Nitrate-Promoted High-Capacity MgO Adsorbents for Regenerable CO_2 Capture at Moderate Temperatures, Chem. Mater. 27 (6) (2015) 1943–1949, https://doi.org/10.1021/cm503295g.

[19] T. Harada, T.A. Hatton, Colloidal Nanoclusters of MgO Coated with Alkali Metal Nitrates/Nitrites for Rapid, High Capacity CO_2 Capture at Moderate Temperature, Chem. Mater. 27 (23) (2015) 8153–8161, https://doi.org/10.1021/acs.chemmater.5b03904.

[20] J.S. Kwak, K.R. Oh, K.Y. Kim, J.M. Lee, Y.U. Kwon, CO_2 absorption and desorption characteristics of MgO-based absorbent promoted by triple eutectic alkali carbonate, Phys. Chem. Chem. Phys. 21 (37) (2019) 20805–20813, https://doi.org/10.1039/c9cp03258d.

[21] H. Cui, Z. Cheng, Z. Zhou, Unravelling the role of alkaline earth metal carbonates in intermediate temperature CO_2 capture using alkali metal salt-promoted MgO-based sorbents, J. Mater. Chem. A 8 (35) (2020) 18280–18291, https://doi.org/10.1039/d0ta06170k.

[22] J. Seongmin, H.o. Keon, L. Chang-Ha, Facile synthesis of hierarchically porous MgO sorbent doped with $CaCO_3$ for fast CO_2 capture in rapid intermediate temperature swing sorption, Chem. Eng. J. 334 (2018) 1605–1613, https://doi.org/10.1016/j.cej.2017.11.095.

[23] X. Zhao, G. Ji, W. Liu, X. He, E.J. Anthony, M. Zhao, Mesoporous MgO promoted with $NaNO_3$/$NaNO_2$ for rapid and high-capacity CO_2 capture at moderate temperatures, Chem. Eng. J. 332 (2017) 216–226, https://doi.org/10.1016/j.cej.2017.09.068.

[24] S. Jin, K.-J. Ko, Y.-G. Song, K. Lee, C.-H. Lee, Fabrication and kinetic study of spherical MgO agglomerates via water-in-oil method for pre-combustion CO_2 capture, Chem. Eng. J. 359 (2019) 285–297.

[25] Y. Hu, Y. Guo, J. Sun, H. Li, W. Liu, Progress in MgO sorbents for cyclic CO_2 capture: a comprehensive review, J. Mater. Chem. A 7 (35) (2019) 20103–20120.

[26] A. Dal Pozzo, A. Armutlulu, M. Rekhtina, P.M. Abdala, C.R. Müller, CO_2 Uptake and Cyclic Stability of MgO-Based CO_2 Sorbents Promoted with Alkali Metal Nitrates and Their Eutectic Mixtures, ACS Applied Energy Materials 2 (2) (2019) 1295–1307, https://doi.org/10.1021/acsaem.8b01852.

[27] V. Hiremath, A.H. Jadhav, H. Lee, S. Kwon, J.G. Seo, Highly reversible CO_2 capture using amino acid functionalized ionic liquids immobilized on mesoporous silica, Chem. Eng. J. 287 (2016) 602–617, https://doi.org/10.1016/j.cej.2015.11.075.

[28] A. Parameswari, Y. Soujanya, G.N. Sastry, Functionalized Rutile TiO_2(110) as a Sorbent To Capture CO_2 through Noncovalent Interactions: a Computational Investigation, The Journal of Physical Chemistry C 123 (6) (2019) 3491–3504, https://doi.org/10.1021/acs.jpcc.8b09311.

[29] H. Zhao, N. Qi, Y. Li, Interaction between polysaccharide monomer and SiO_2/Al_2O_3/$CaCO_3$ surfaces: a DFT theoretical study, Appl. Surf. Sci. 466 (2019) 607–614, https://doi.org/10.1016/j.apsusc.2018.10.085.

[30] K. Zhang, X.S. Li, W.-Z. Li, A. Rohatgi, Y. Duan, P. Singh, L. Li, D.L. King, Phase Transfer-Catalyzed Fast CO_2 Absorption by MgO-Based Absorbents with High Cycling Capacity, Adv. Mater. Interfaces 1 (3) (2014) 1400030, https://doi.org/10.1002/admi.201400030.

[31] X. Ge, L. Yin, S-doping induced boosted electrochemical redox kinetics in Te1-xSx nanorod cathodes for high volumetric capacity Li-Te batteries, Energy Storage Mater. 20 (2019) 89–97, https://doi.org/10.1016/j.ensm.2019.05.012.

[32] D. Bielsa, A. Zaki, P.L. Arias, A. Faik, Improving the redox performance of Mn_2O_3/Mn_3O_4 pair by Si doping to be used as thermochemical energy storage for concentrated solar power plants, Sol. Energy 204 (2020) 144–154, https://doi.org/10.1016/j.solener.2020.04.073.

[33] L. Wang, Z. Zhou, Y. Hu, Z. Cheng, X. Fang, Nanosheet MgO-Based CO_2 Sorbent Promoted by Mixed-Alkali-Metal Nitrate and Carbonate: performance and Mechanism, Ind. Eng. Chem. Res. 56 (20) (2017) 5802–5812, https://doi.org/10.1021/acs.iecr.7b00483.

[34] L. Zhang, X. Huang, C. Qin, K. Brinkman, Y. Gong, S. Wang, K. Huang, First spectroscopic identification of pyrocarbonate for high CO_2 flux membranes containing highly interconnected three dimensional ionic channels, Phys. Chem. Chem. Phys. 15 (31) (2013) 13147–13152, https://doi.org/10.1039/c3cp52362d.